Accurate Single-Valued Double Many-Body Expansion Potential Energy Surface for Ground-State HN$_2$
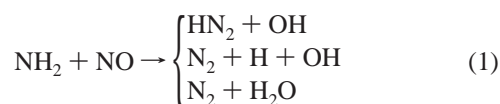
L. A. Poveda and A. J. C. Varandas*

Departamento de Química, Universidade de Coimbra, 3004-535 Coimbra, Portugal

Received: May 5, 2003; In Final Form: July 11, 2003

A single-valued double many-body expansion potential energy surface is reported for ground-state HN$_2$ by fitting accurate ab initio energies that have been suitably corrected by scaling for the H−N$_2$ and N−NH regions. The energies of ∼900 geometries have been calculated at the multireference configuration interaction level, using aug-cc-pVQZ basis sets of Dunning and the full valence complete active space wave function as reference. The topographical features of the novel global potential energy surface are examined in detail.

1. Introduction

Several experimental and theoretical studies have attempted to elucidate the possible role of the HN$_2$ species as a critical step in various reactions. Although this molecule has never been observed experimentally, it has been postulated to be an important intermediary in thermal De−NO$_x$ processes,[1,2] with indirect evidence that suggests its existence through the three possible product channels proposed for the NH$_2$ + NO reaction:

$$\text{NH}_2 + \text{NO} \rightarrow \begin{cases} \text{HN}_2 + \text{OH} \\ \text{N}_2 + \text{H} + \text{OH} \\ \text{N}_2 + \text{H}_2\text{O} \end{cases} \qquad (1)$$

The experiments that are focused to determine the rate coefficient and the major pathway of reaction 1 are far from consistent: although the experimental studies vary widely, in regard to the branching ratio for OH production, none of the experiments observed H atoms.[3] This result, along with the assumed product channels, argues for the existence of the HN$_2$ species. However, a controversy persists from the kinetics modeling studies.[2,4] In fact, although an estimate of 10^{-4} s for the lifetime produces a reasonable match to experimental observations, the theoretical studies of HN$_2$ unimolecular decay predict a much shorter value, of 10^{-8}−10^{-9} s, for the ground vibrational state.[5−7]

Many ab initio studies of the reaction

$$\text{H} + \text{N}_2 \rightarrow \text{HN}_2 \qquad (2)$$

have previously been made to characterize the geometry and energetics of the reactants, transition state, and products.[3] All previous calculations concluded that the title system is quasibound (the global minimun is located above the H + N$_2$ asymptote) with a barrier height to dissociation of ∼11 kcal/mol. From such studies, a global potential energy surface was reported by Walch[5,8,9] and Koizumi et al.[6] for the H + N$_2$ channel. On the basis of a spline fit of the ab initio points calculated using the completed active space self-consistent field/externally contracted configuration interaction (CASSCF/CCI) method and two different basis sets, Walch and co-workers

predicted, depending on the basis set used, a barrier height of 10.2 or 11.3 kcal/mol and a global minimum of 5.6 or 3.9 kcal/mol above the H + N$_2$ asymptote.

In a subsequent paper,[10] Walch and Partidge attempted a conclusive and accurate prediction of the HN$_2$ unimolecular decomposition. They reported a systematic study of the HN$_2$ energetics using the complete active space self-consistent field/internally contracted configuration interaction (CASSCF/ICCI) method and the cc-pVDZ, cc-pVTZ, cc-pVQZ, and cc-pV5Z basis sets of Dunning.[11,12] From such results, an extrapolation to the complete basis set limit has been obtained, which yields a barrier height of 11.34 kcal/mol and a global minimum 4.31 kcal/mol above the H + N$_2$ asymptote. A slight difference between the constrained minimum path calculated at this level of theory and the one previously estimated using a potential energy surface[6] induced those authors to conclude "...we are very confident of the theoretical lifetime predictions for the HN$_2$ radical".

In a more recent publication, Gu et al.[13] reported a high level CCSD(T)/aug-cc-pVQZ calculation of the stationary points for the title system. They predict the classical barrier height for the reaction HN$_2$ → H + N$_2$ to be 10.7 kcal/mol, thus lying 0.6 kcal/mol below the extrapolated value reported by Walch and Partidge.[10] In turn, the calculated[13] exothermicity for the reaction H + N$_2$ → HN$_2$ is 3.8 kcal/mol, which is, thus, slightly smaller than the extrapolated value[10] of 4.31 kcal/mol. We may therefore argue that there is not a conclusive result yet for the HN$_2$ lifetime.

In this work, we report the first realistic global potential energy surface for the ground electronic state of the title system, based on the double many-body expansion[14−17] (DMBE) method. Being a potential fragment of larger N$_x$H$_y$ species, such as those of relevance in studying the synthesis of ammonia, it may also be of crucial importance in constructing the corresponding global DMBE forms for larger hydrogen−nitrogen polyatomic species. Indeed, this has been a major motivation for the present work. Specifically, the analytic HN$_2$ DMBE potential energy surface will be calibrated from ∼900 ab initio points that were calculated at the multireference configuration interaction (MRCI) level, using the full valence complete active space (FVCAS) reference function and the aug-cc-pVQZ (AVQZ) Dunning[11,12] basis set. The ab initio energies calculated in this way have been subsequently corrected, using the double

* Author to whom correspondence should be addressed. E-mail address: varandas@qtvs1.qui.uc.pt.

many-body expansion−scaled external correlation[18] (DMBE−SEC) method to extrapolate to the complete basis set/complete configuration interaction limits. As usual in DMBE theory,[14−17] the potential energy surface so obtained shows the correct long-range behavior at all dissociation channels while providing a realistic representation of the surface features at all interatomic separations (e.g., van der Waals wells at intermediate atom−diatom separations).

The paper is organized as follows. Section 2 describes the ab initio calculations that have been performed in the present work. In Section 3, we examine the analytical representation of the potential energy surface; specifically, Section 3.1 focuses on the two-body energy terms, whereas Section 3.2 concentrates on the three-body energy terms. The main topographical features of the DMBE potential energy surface are discussed in Section 4. Some concluding remarks are given in Section 5.

2. Ab Initio Calculations

The ab initio caluclations have been performed at the MRCI[19] level, using the FVCAS[20] wave function as reference. This involves nine active orbitals ($7a' + 2a''$), with the nitrogen $1s$ orbitals forming the $1a'$ and $2a'$ molecular orbitals, having been left uncorrelated. Such a FVCAS reference wave function represents a total of 3080 configuration state functions. For the basis set, we have selected the aug-cc-pVQZ (AVQZ) of Dunning,[11,12] with the correlated ab initio calculations being performed using the MOLPRO[21] package. Approximately 900 grid points have been computed to map the potential energy surface over the region defined by $1.6 \leq R_{N_2}/a_0 \leq 2.8$, $1.5 \leq r_{H-N_2}/a_0 \leq 10.0$, and $0.0 \leq \gamma \leq 90°$ for H−N_2 interactions, and $1.5 \leq R_{NH}/a_0 \leq 2.4$, $1.5 \leq r_{N-NH}/a_0 \leq 6.0$, and $0.0 \leq \gamma \leq 180°$ for N − NH interactions; r, R, and γ are the corresponding atom−diatom Jacobi coordinates.

The ab initio energies calculated in this way have been subsequently corrected using the DMBE−SEC[16] method to account for the excitations beyond singles and doubles and, most importantly, for the incompleteness of the basis set. Thus, the total DMBE−SEC interaction energy is written as

$$V(\mathbf{R}) = V_{FVCAS}(\mathbf{R}) + V_{SEC}(\mathbf{R}) \tag{3}$$

where

$$V_{FVCAS}(\mathbf{R}) = \sum_{AB} V^{(2)}_{AB,FVCAS}(R_{AB}) + V^{(3)}_{ABC,FVCAS}(R_{AB}, R_{BC}, R_{AC}) \tag{4}$$

and

$$V_{SEC}(\mathbf{R}) = \sum_{AB} V^{(2)}_{AB,SEC}(R_{AB}) + V^{(3)}_{ABC,SEC}(R_{AB}, R_{BC}, R_{AC}) \tag{5}$$

where $\mathbf{R} = \{\mathbf{R}_i\}$ is a collective variable of all internuclear distances. In turn, the first two terms of the SEC series expansion assume the form

$$V^{(2)}_{AB,SEC}(R_{AB}) = \frac{V^{(2)}_{AB,FVCAS-CISD}(R_{AB}) - V^{(2)}_{AB,FVCAS}(R_{AB})}{F^{(2)}_{AB}} \tag{6}$$

$$V^{(3)}_{ABC,SEC}(R_{AB}, R_{BC}, R_{AC}) = \frac{V^{(3)}_{ABC,FVCAS-CISD}(R_{AB}, R_{BC}, R_{AC}) - V^{(3)}_{ABC,FVCAS}(R_{AB}, R_{BC}, R_{AC})}{F^{(3)}_{ABC}} \tag{7}$$

Following previous work,[16] the $F^{(2)}_{AB}$ parameter in eq 6 has been chosen to reproduce the bond dissociation energy of the corresponding AB diatomic, while $F^{(3)}_{ABC}$ has been estimated as the average of the two-body F-factors. Such a procedure leads to the following values: $F^{(2)}_{NN} = 0.758$, $F^{(2)}_{NH} = 0.948$, and $F^{(3)}_{NNH} = 0.885$.

3. Double Many-Body Expansion Potential Energy Surface

3.1. Two-Body Energy Terms. The diatomic potential curves have been modeled using the extended Hartree−Fock approximate correlation energy method for diatomic molecules, including the united atom limit[22] (EHFACE2U), with the available parameters being determined by fitting experimental and ab initio data. Thus, they assume the general form[15,22]

$$V = V_{EHF}(R) + V_{dc}(R) \tag{8}$$

where the label EHF refers to the extended Hartree−Fock type energy and the label dc indicates the dynamical correlation energy. As usual, the latter is modeled semiempirically by[23]

$$V_{dc}(R) = -\sum_{n=6,8,10} C_n \chi_n(R) R^{-n} \tag{9}$$

with the damping function for the dispersion coefficients assuming the form

$$\chi_n(R) = \left[1 - \exp\left(-A_n \frac{R}{\rho} - B_n \frac{R^2}{\rho^2}\right)\right]^n \tag{10}$$

In eq 10, A_n and B_n are auxiliary functions that are defined by

$$A_n = \alpha_0 n^{-\alpha_1} \tag{11}$$

$$B_n = \beta_0 \exp(-\beta_1 n) \tag{12}$$

where α_0, β_0, α_1, and β_1 are universal dimensionless parameters for all isotropic interactions:[14,15] $\alpha_0 = 16.36606$, $\alpha_1 = 0.70172$, $\beta_0 = 17.19338$, and $\beta_1 = 0.09574$. In turn, the scaling parameter ρ is defined as

$$\rho = 5.5 + 1.25 R_0 \tag{13}$$

where $R_0 = 2(\langle r_A^2 \rangle^{1/2} + \langle r_B^2 \rangle^{1/2})$ is the LeRoy[24] parameter for onset the undamped R^{-n} expansion, and $\langle r_X^2 \rangle$ is the expectation value of the squared radius for the outermost electrons of atom X (where X = A, B). Finally, the exponential decaying portion of the EHF-type energy term assumes the general form

$$V_{EHF}(R) = -\frac{D}{R}\left(1 + \sum_{i=1}^{n} a_i r^i\right) \exp(-\gamma r) \tag{14}$$

where

$$\gamma = \gamma_0[1 + \gamma_1 \tanh(\gamma_2 r)] \tag{15}$$

$r = R - R_e$ is the displacement from the equilibrium diatomic geometry, and D and a_i ($i = 1,..., n$) are adjustable parameters to be obtained as described elsewhere.[15,22] Specifically, the potential curve of ground-state $N_2(X^1\Sigma^+)$ has been calibrated by fitting simultaneously vibrational frequencies, Rydberg−Kleing−Rees (RKR) turning points,[25] and the ab initio energies calculated in the present work for the repulsive wing. Figure 1 shows that the final potential curve reproduces our calculated
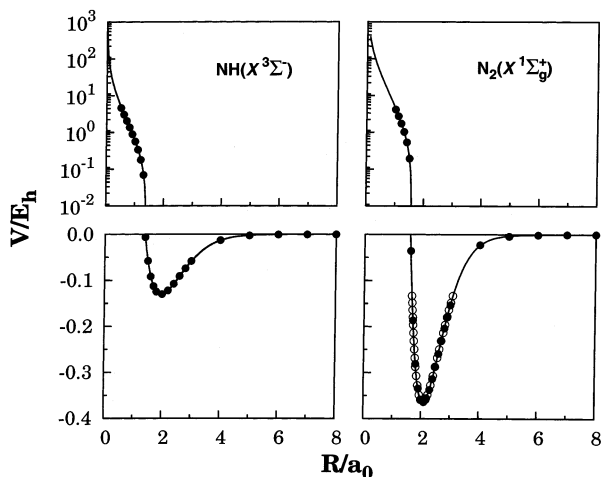
DMBE Potential Energy Surface for Ground-State HN₂

J. Phys. Chem. A, Vol. 107, No. 39, 2003 **7925**

Figure 1. EHFACE2U potential energy curves for NH($^3\Sigma^-$) and N₂($^1\Sigma_g$). Key for symbols: (○) Rydberg−Kleing−Ress (RKR) data and (●) ab initio points.

TABLE 1: Parameters in the Two-Body Energy Curves

	NH(X$^3\Sigma^-$)	N₂(X$^1\Sigma_g^+$)
R_e (a_0)	1.9650	2.0743
D (E_h)	0.229 034 01	0.702 119 20
a_1 (a_0^{-1})	2.146 641 73	2.211 672 95
a_2 (a_0^{-2})	0.844 712 52	0.991 485 45
a_3 (a_0^{-3})	0.525 908 29	1.553 769 29
γ_0 (a_0^{-1})	1.563 792	1.678 669
γ_1 (a_0^{-1})	0.661 116	0.674 118
γ_2 (a_0^{-1})	0.282 985	0.716 957
R_0 (a_0)	6.7560	6.5938
$C_6/(E_h a_0^{-6})$	12.27	22.8
$C_8/(E_h a_0^{-8})$	232.6	442.6
$C_{10}/(E_h a_0^{-10})$	5775	9722

ab initio energies. In turn, for ground-state imidogen, NH(X$^3\Sigma^-$), we have used a previously reported potential energy curve[26] calibrated from the MRCI+Q ab initio points of Stallcop et al.[27] The numerical values of all the parameters are, for both diatomic potentials, gathered in Table 1.

3.2. Three-Body Energy Terms. In regard to the two-body energies, the three-body energy splits into several contributions. First, the three-body energy is divided into an extended Hartree−Fock part and a dynamical correlation part. For the three-body dynamical correlation, we select the form that was proposed elsewhere by one of us[28] for the water molecule, namely

$$V_{dc}^{(3)} = \sum_i \sum_n f_i(\mathbf{R}) C_n^{(i)}(R_i, \theta_i) \chi_n(r_i) r_i^{-n} \tag{16}$$

where the i label represents the I−JK channel associated with the center of mass separation r_i, R_i is the J−K bond distance, and $\cos \theta_i = \vec{r}_i \vec{R}_i / |\vec{r}_i \vec{R}_i|$. (For the notation, see Figure 1 of ref 16.) For $n = 6$, 8, and 10, $C_n^{(i)}(R_i, \theta_i)$ are atom−diatom dispersion coefficients, which are given by

$$C_n^{(i)} = \sum_L C_n^L P_L(\cos \theta_i) \tag{17}$$

where $P_L(\cos \theta_i)$ denotes the L-th term of the Legendre polynomial expansion. In addition, the function $\chi_n(r_i)$ in eq 16 is the corresponding diatomic damping function. Moreover, $f_i(\mathbf{R})$ is a switching function that is chosen from the requirement that

its value must be +1 at $R_i = R_i^e$ and $r_i \to \infty$, and 0 when $R_i \to \infty$. One such form is[28]

$$f_i = \frac{1}{2}\{1 - \tanh[\xi(\eta s_i - s_j - s_k)]\} \tag{18}$$

where $s_i = R_i - R_i^e$ (corresponding expressions apply to s_j, s_k, f_j, and f_k) and η is a constant that is chosen to ensure the proper asymptotic behavior. Following previous work,[28] we adopt a value of $\eta = 3$. In addition, the parameter ξ has been assumed to be equal to 1.0 a_0^{-1}. Regarding the damping function $\chi_n(r_i)$, we still adopt eq 10 but replace R by the center-of-mass separation for the relevant atom−diatom channel. In addition, the value of ρ has been assumed by considering R_0 in eq 13 as the average of the LeRoy parameters for NO and SiH, which leads to a value of $\rho = 15.9$.

3.3. Three-Body Dynamical Correlation Energy. The $L = 0$, 2, and 4 components of the atom−diatom dispersion coefficients have been considered, with the involved internuclear dependences being estimated as reported elsewhere,[29] i.e., using the dipolar polarizabilities calculated in the present work at the MRCI level of theory jointly with the generalized Slater−Kirkwood approximation.[30] The atom−diatom dispersion coefficients thus calculated were then fitted to the form

$$C_n^{A-BC}(R) =$$
$$C_n^{AB} + C_n^{AC} + D_M(1 + \sum_{i=1}^3 a_i r^i) \exp(-a_1 r - \sum_{i=2}^3 b_i r^i) \tag{19}$$

where $r = R - R_M$ is the displacement relative to the position of the maximum. The parameters that resulted from such fits are reported in Table 2, whereas the internuclear dependences of the dispersion coefficients are shown in Figure 2.

As noted elsewhere,[28] eq 16 causes an overestimation of the dynamical correlation energy at the atom−diatom dissociation channels. To correct such a behavior, we have multiplied the two-body dynamical correlation energy for the i-th pair by $f_i(\mathbf{R})$ and correspondingly for channels j and k. This ensures[28] that the only two-body contribution at the i-th channel is that of JK.

3.4. Three-Body Extended Hartree−Fock Energy. By removing, for a given triatomic geometry, the sum of the two-body energy terms from the corresponding DMBE−SEC interaction energies (eq 3), which was defined with respect to the infinitely separated ground-state atoms, one obtains the total three-body energy. Therefore, by subtracting the three-body dynamical correlation contribution (eq 16) from the total three-body energy that is calculated in that way, one obtains the three-body extended Hartree−Fock energy contribution. To represent the latter, we use the following three-body distributed-polynomial[31] form:

$$V_{EHF}^{(3)} = \sum_{j=1}^5 P^{(j)}(Q_1, Q_2, Q_3) \prod_{i=1}^3 \{1 - \tanh[\gamma_i^j(R_i - R_i^{j,ref})]\} \tag{20}$$

where $P^{(j)}(Q_1, Q_2, Q_3)$ is the j-th polynomial. To the sixth order, this assumes the form

Figure 2. Dispersion coefficients for atom−diatom asymptotic channels of HN$_2$, as a function of the corresponding internuclear distance *R*.

Figure 3. Reference geometries (with distances in atomic units, a.u.) for the three-body EHF portion of the potential energy surface. See text for details.

$$P^j(Q_1, Q_2, Q_3) = c_1 + c_2 Q_1 + c_3 Q_3 + c_4 Q_1^2 + c_5 S_{2a}^2 +$$
$$c_6 Q_1 Q_3 + c_7 S_{2b}^2 + c_8 Q_1^3 + c_9 Q_1 S_{2a}^2 + c_{10} S_3^3 + c_{11} Q_1^2 Q_3 +$$
$$c_{12} Q_1 S_{2b}^2 + c_{13} Q_3 S_{2a}^2 + c_{14} Q_1^4 + c_{15} Q_1^2 S_{2a}^2 + c_{16} S_{2a}^4 +$$
$$c_{17} Q_1 S_3^3 + c_{18} Q_1^3 Q_3 + c_{19} Q_1^2 S_{2b}^2 + c_{20} Q_1 Q_3 S_{2a}^2 + c_{21} Q_3 S_3^3 +$$
$$c_{22} S_{2a}^2 S_{2b}^2 + c_{23} Q_1^5 + c_{24} Q_1^3 S_{2a}^2 + c_{25} Q_1 S_{2a}^4 + c_{26} Q_1^2 S_3^3 +$$
$$c_{27} S_{2a}^2 S_3^3 + c_{28} Q_1^4 Q_3 + c_{29} Q_1^3 S_{2b}^2 + c_{30} Q_1^2 Q_3 S_{2a}^2 +$$
$$c_{31} Q_1 Q_3 S_3^3 + c_{32} Q_1 S_{2a}^2 S_{2b}^2 + c_{33} Q_3 S_{2a}^4 + c_{34} S_{2b}^2 S_3^3 + c_{35} Q_1^6 +$$
$$c_{36} Q_1^4 S_{2a}^2 + c_{37} Q_1^2 S_{2a}^4 + c_{38} Q_1^3 S_3^3 + c_{39} Q_1 S_{2a}^2 S_3^3 + c_{40} S_{2a}^6 +$$
$$c_{41} S_3^6 + c_{42} Q_1^5 Q_3 + c_{43} Q_1^4 S_{2b}^2 + c_{44} Q_1^3 Q_3 S_{2a}^2 + c_{45} Q_1^2 Q_3 S_3^3 +$$
$$c_{46} Q_1^2 S_{2a}^2 S_{2b}^2 + c_{47} Q_1 Q_3 S_{2a}^4 + c_{48} Q_1 S_{2b}^2 S_3^3 + c_{49} Q_3 S_{2a}^2 S_3^3 +$$
$$c_{50} S_{2a}^4 S_{2b}^2 \quad (21)$$

where $S_{2a}^2 = Q_2^2 + Q_3^2$, $S_{2b}^2 = Q_2^2 - Q_3^2$, and $S_3^3 = Q_3^3 - 3Q_2^2 Q_3$, with Q_i ($i = 1-3$) being symmetry coordinates that are defined, for the *j*-th polynomial, by

$$\begin{pmatrix} Q_1 \\ Q_2 \\ Q_3 \end{pmatrix} = \begin{pmatrix} \sqrt{\frac{1}{3}} & \sqrt{\frac{1}{3}} & \sqrt{\frac{1}{3}} \\ 0 & \sqrt{\frac{1}{2}} & -\sqrt{\frac{1}{2}} \\ \sqrt{\frac{2}{3}} & -\sqrt{\frac{1}{6}} & -\sqrt{\frac{1}{6}} \end{pmatrix} \begin{pmatrix} R_1 - R_1^{j,\text{ref}} \\ R_2 - R_2^{j,\text{ref}} \\ R_3 - R_3^{j,\text{ref}} \end{pmatrix} \quad (22)$$

where the superscript "ref" means a reference geometry. Figure 3 displays the reference geometries that are used to define the displacement coordinates used to write the five EHF-type polynomials in eq 20. Note that the first and second polynomials (which refer to the first and second sets of coefficients in Table 3) are respectively centered in structures a) and b) of Figure 3. In turn, two other polynomials use the same set of coefficients (the third column of Table 3), which are centered in structure c) of Figure 3. The last polynomial, $P^{(5)}(Q_1, Q_2, Q_3)$, is centered at reference geometry d) in Figure 3, which lies close to the equilibrium structure of the weakly bound H$\cdots$N$_2$ van der Waals species. Note that this includes up to cubic terms only, because this proved to be sufficient for our fitting purposes. To obtain $R_i^{j,\text{ref}}$, we have first assumed their values to coincide with the

TABLE 2: Numerical Values of the Parameters in eq 19

	$C_6^0(R)$	$C_6^2(R)$	$C_8^0(R)$	$C_8^2(R)$	$C_8^4(R)$	$C_{10}^0(R)$
			H−N$_2$			
R_M (a_0)	3.5667	3.5090	3.5026	3.4863	3.4870	3.4608
D_M (E_h)	4.7294	3.7419	178.7058	298.9732	22.9832	7028.8116
a_1 (a_0^{-1})	1.277 799 82	0.851 582 13	1.131 083 35	0.884 602 42	0.879 306 21	1.090 186 28
a_2 (a_0^{-2})	0.300 410 55	0.184 349 94	0.277 939 09	0.196 563 42	0.198 953 65	0.275 794 87
a_3 (a_0^{-3})	−0.003 100 54	−0.000 969 88	−0.000 106 74	−0.000 933 54	0.000 965 52	0.001 704 86
b_2 (a_0^{-2})	0.315 677 76	0.269 098 43	0.135 718 43	0.293 195 75	0.945 261 28	0.096 086 57
b_3 (a_0^{-3})	0.047 870 65	0.028 844 54	0.009 978 24	0.044 310 67	0.216 377 09	0.006 945 65
			N−NH			
R_M (a_0)	3.4400	3.2316	3.4371	3.2506	3.2187	3.4352
D_M (E_h)	5.8549	5.5978	143.9529	379.7076	31.0459	4394.6574
a_1 (a_0^{-1})	1.595 253 94	1.026 484 21	1.584 495 87	0.931 566 40	1.644 505 86	−0.073 743 22
a_2 (a_0^{-2})	0.708 758 04	0.270 832 16	0.703 651 10	0.182 778 32	0.86 5513 27	−0.607 106 28
a_3 (a_0^{-3})	0.104 478 27	0.015 983 88	0.103 522 65	−0.001 626 53	0.139 612 00	0.497 138 66
b_2 (a_0^{-2})	0.284 813 14	0.270 234 30	0.289 780 70	0.318 737 43	0.684 793 26	0.553 195 06
b_3 (a_0^{-3})	1.0×10^{-8}	1.0×10^{-8}	1.0×10^{-8}	1.0×10^{-8}	1.0×10^{-8}	0.106 836 28

TABLE 3: Numerical Values of the Extended Hartree−Fock Energy (eq 20)

coefficient	$P^{(1)}$	$P^{(2)}$	$P^{(3)} + P^{(4)}$	$P^{(5)}$
$c_1\ (a_0^0)$	−35.35722711	50.89357137	0.64204663	−0.00037787
$c_2\ (a_0^{-1})$	1.43122305	−8.20511664	−1.57901897	−0.00190090
$c_3\ (a_0^{-1})$	−9.87617675	−44.75381891	−0.94137581	−0.00261274
$c_4\ (a_0^{-2})$	−18.80416915	26.48543000	1.81933025	0.00029084
$c_5\ (a_0^{-2})$	−21.78867083	32.57491690	0.60735250	−0.00057451
$c_6\ (a_0^{-2})$	−11.07940674	−33.13037794	0.52335000	−0.00038871
$c_7\ (a_0^{-2})$	5.01128977	5.08772061	0.25855378	0.00055106
$c_8\ (a_0^{-3})$	0.96613480	−3.99536563	−1.18504903	0.
$c_9\ (a_0^{-3})$	−0.77697807	10.11891334	−0.63735021	−0.00076654
$c_{10}\ (a_0^{-3})$	−0.92099871	4.10517993	0.12413155	0.
$c_{11}\ (a_0^{-3})$	−6.01375589	−16.78809143	−0.38833222	−0.00104352
$c_{12}\ (a_0^{-3})$	0.90509055	−16.20351814	0.11928222	0.00074255
$c_{13}\ (a_0^{-3})$	−5.14061355	−17.17930402	−0.82128727	0.
$c_{14}\ (a_0^{-4})$	−3.40765945	3.78922878	0.63973511	0.
$c_{15}\ (a_0^{-4})$	−1.88077926	3.13322630	−0.26288962	0.
$c_{16}\ (a_0^{-4})$	−2.68379376	5.69616150	0.17067403	0.
$c_{17}\ (a_0^{-4})$	4.45588653	−5.81699928	−0.18560723	0.
$c_{18}\ (a_0^{-4})$	−4.05543497	−7.84835242	0.12054093	0.
$c_{19}\ (a_0^{-4})$	1.70217322	−11.08806364	−0.17812786	0.
$c_{20}\ (a_0^{-4})$	−3.39696345	−5.64359911	0.34470547	0.
$c_{21}\ (a_0^{-4})$	0.52809629	1.62229042	−0.24358630	0.
$c_{22}\ (a_0^{-4})$	0.96757611	1.49907056	0.29036290	0.
$c_{23}\ (a_0^{-5})$	0.07042292	−0.52463644	−0.18613603	0.
$c_{24}\ (a_0^{-5})$	−1.13489314	2.85006561	0.39057365	0.
$c_{25}\ (a_0^{-5})$	1.21500520	0.84486292	−0.10864732	0.
$c_{26}\ (a_0^{-5})$	0.90416261	−3.39970612	−0.08699980	0.
$c_{27}\ (a_0^{-5})$	−0.37424676	0.07267052	−0.09095443	0.
$c_{28}\ (a_0^{-5})$	−1.41649184	−0.91682855	−0.10631151	0.
$c_{29}\ (a_0^{-5})$	−0.04756769	−1.68254925	0.26417945	0.
$c_{30}\ (a_0^{-5})$	0.61305975	−3.72605017	0.33025474	0.
$c_{31}\ (a_0^{-5})$	1.84502268	3.16507583	0.00837542	0.
$c_{32}\ (a_0^{-5})$	−0.58400452	−1.42401824	−0.07300291	0.
$c_{33}\ (a_0^{-5})$	−0.13609210	−2.12175750	−0.21211357	0.
$c_{34}\ (a_0^{-5})$	−0.05015587	1.04011399	0.23138290	0.
$c_{35}\ (a_0^{-6})$	−0.12738976	0.02661556	0.03395371	0.
$c_{36}\ (a_0^{-6})$	0.62237114	−0.02032757	−0.18379018	0.
$c_{37}\ (a_0^{-6})$	0.10324812	0.78316160	0.05864884	0.
$c_{38}\ (a_0^{-6})$	−0.42328134	−0.45490030	−0.05717854	0.
$c_{39}\ (a_0^{-6})$	0.76664528	−0.77298638	0.03477564	0.
$c_{40}\ (a_0^{-6})$	−0.21436778	0.45857204	0.00603242	0.
$c_{41}\ (a_0^{-6})$	−0.03021494	0.16268811	−0.04950996	0.
$c_{42}\ (a_0^{-6})$	−0.17424122	0.08238406	−0.03113967	0.
$c_{43}\ (a_0^{-6})$	0.10050895	−0.35417930	0.04913502	0.
$c_{44}\ (a_0^{-6})$	0.61827911	−1.07342606	−0.00694684	0.
$c_{45}\ (a_0^{-6})$	0.42896861	1.11079450	0.04085605	0.
$c_{46}\ (a_0^{-6})$	−0.37356092	−0.70735541	−0.27048435	0.
$c_{47}\ (a_0^{-6})$	0.29520788	−1.15920924	−0.04881234	0.
$c_{48}\ (a_0^{-6})$	−0.37797059	0.53374300	−0.18376155	0.
$c_{49}\ (a_0^{-6})$	0.23373482	0.20831280	0.02121087	0.
$c_{50}\ (a_0^{-6})$	0.16170869	−0.34419861	0.15943928	0.
$\gamma_1^j\ (a_0^{-1})$	1.30	0.40	1.55	1.00
$\gamma_2^j\ (a_0^{-1})$	1.10	1.35	−0.55[a]	0.35
$\gamma_3^j\ (a_0^{-1})$	1.10	1.35	1.55[a]	0.35
$R_1^{j,\mathrm{ref}}\ (a_0)$	2.00	2.60	2.05	2.08
$R_2^{j,\mathrm{ref}}\ (a_0)$	2.50	2.05	1.95[b]	7.00
$R_3^{j,\mathrm{ref}}\ (a_0)$	2.50	2.05	4.00[b]	7.00

[a] The values indicated should be interchanged when writing polynomials P^3 and P^4. [b] See footnote a.

bond distances of the associated stationary points, and, subsequently, relaxed this condition via a trial-and-error least-squares
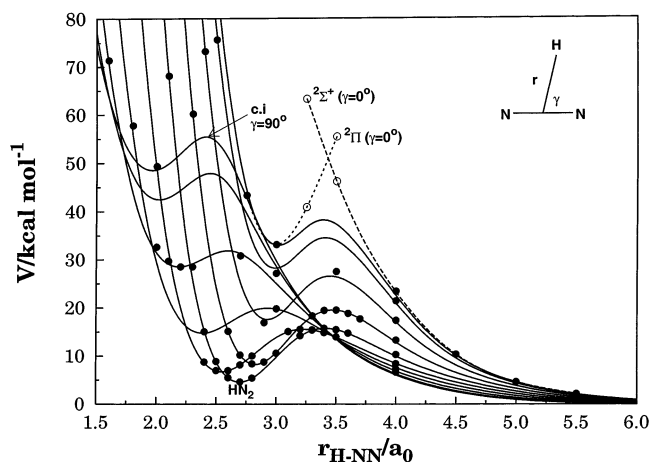

Figure 4. Selected cuts of the HN$_2$ potential energy surface. The figure shows 10 minimum energy cuts for fixed values of γ as a function of the distance r_{H-N_2}. Note the avoided crossing for T-shaped and linear configurations. Unfilled points correspond to geometries close to the conical intersection, which have not been included in the least-squares fitting procedure.

TABLE 4: Stratified Root-Mean-Square Deviations

energy (kcal/mol)	number of points	maximum deviation (kcal/mol)	rmsd[a]
20	224	0.90	0.152
40	308	2.36	0.256
60	540	9.06	0.620
80	570	9.06	0.714
100	597	9.06	0.765
200	825	10.06	0.935
300	887	10.06	0.982
500	913	10.06	1.070

[a] Root-mean-square deviation.

fitting procedure. The nonlinear range-determining parameters γ_i^j have been optimized in a similar way. Thus, the complete set of parameters totals 160 linear coefficients c_i, 15 nonlinear coefficients γ_i^j, and 15 reference geometries $R_i^{j,\mathrm{ref}}$. Their optimal numerical values are collected in Table 3. A total of 913 points have been used for the calibration procedure, with the energies covering a range up to 500 kcal/mol above the H + N$_2$ asymptote.

Table 4 shows the stratified root-mean-square deviation (rmsd) values of the final potential energy surface, with respect to the fitted and nonfitted ab initio energies. This table shows that the final potential energy surface is able to fit the region of major chemical interest (308 ab initio points with energies up to 40 kcal/mol) with a high accuracy (rmsd = 0.256 kcal/mol). This region includes the global minimum and the transition state for the H + N$_2$ dissociation process. The major deviations correspond to points close to the conical intersection (thus, they have not been included in the fitting procedure, to warrant a behavior of the final single-valued form that is as smooth as possible) and at high repulsive regions of the potential surface. Clearly, the DMBE potential energy surface that has been obtained in this way accurately reproduces all fitted and nonfitted ab initio points, up to 500 kcal/mol.

Figure 4 illustrates the quality of the final fitted form. The profiles correspond to minimum energy cuts for 10 distinct values of γ, whereas the displayed ab initio points form a small set of the total number of points used in the fitting procedure; they have been calculated by optimizing R_{N_2} at specified values of γ and r_{H-N_2}. The two conical intersections that result for T-shaped and linear configurations are clearly visible in Figure
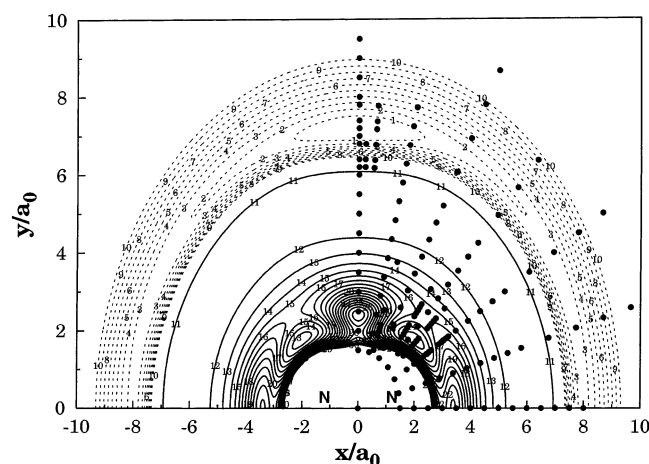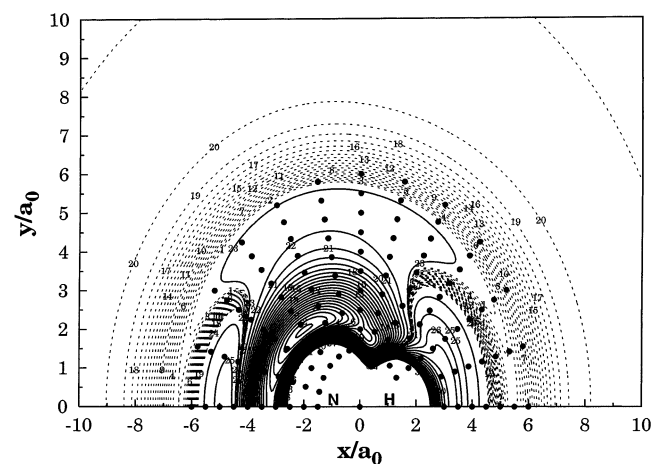
Figure 5. Isoenergy contour plot for a H atom moving around a partially relaxed N_2 diatomic (1.8 $a_0 \leq R_{N_2} \leq$ 2.4 a_0), which lies along the x-axis with the center of the bond fixed at the origin. Contours are equally spaced by 0.005E_h, starting at −0.3640E_h. Contours in dashed lines emphasize the van der Waals minimum; they are equally spaced by 0.000005E_h, starting at −0.36414E_h. Also shown are the calculated ab initio points for the H atom moving around N_2 diatomic, whose bond distance varied over a range from 1.6 a_0 to 2.8 a_0.

Figure 6. Isoenergy contour plot for a N atom moving around a partially relaxed NH diatomic (1.8 $a_0 \leq R_{NH} \leq$ 2.3 a_0), which lies along the x-axis with the center of the bond fixed at the origin. Contours are equally spaced by 0.01 E_h, starting at −0.355 E_h. The contours in dashed are equally spaced by 0.0002 E_h, starting at −0.1340 E_h. Also shown are the calculated ab initio points for the N atom around a NH diatomic, whose bond distance varied over a range from 1.5 a_0 to 2.4 a_0.

4. We emphasize that the regions close to such topological features are smoothed out (i.e., they resemble avoided intersections) in the single-valued representation used in the present work. Thus, the points close to the actual crossing seam (indicated in the plot as unfilled circles) have not been included in the fitting procedure, to avoid spoiling its quality at the regions of more chemical interest.

4. Major Features of Potential Energy Surface

Figures 5 and 6 illustrate the major topographical features of the HN$_2$ DMBE potential energy surface that has been calculated in the present work. Specifically, Figure 5 shows energy contours for a H atom moving around a N$_2$ ground-state diatomic whose bond length is partially relaxed for each position of the H atom. The corresponding plot for a N atom moving around NH is presented in Figure 6. The salient features from these plots are some of the most relevant stationary points for the
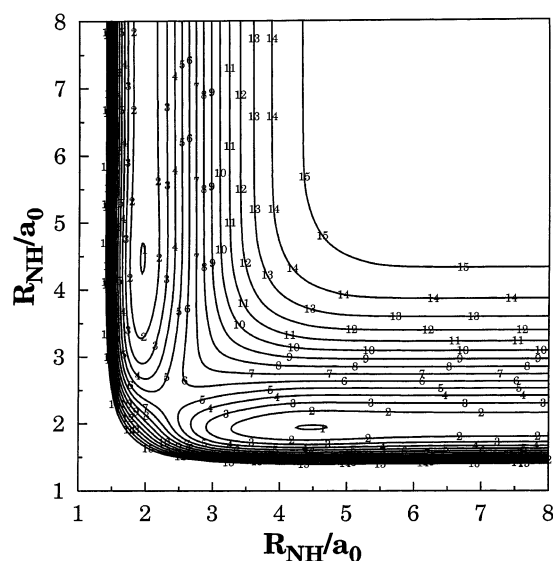

Figure 7. Isoenergy contour plot for the stretching of the two NH bonds in linear N−H−N. Contours are equally spaced by 0.009 E_h, starting at −0.1335 E_h. The two equivalent structures NH⋯N and N⋯HN indicate linear transition states, which appear as hydrogen-bonded minima, with respect to the stretching coordinate (see text).

TABLE 5: Stationary Points of the DMBE Potential Energy Surface, for Various Features

property	MRCI[a]	CASSCF/CCI[b]	PES[c]	DMBE[d]
		Global Minimun		
R_1 (a_0)	2.227	2.253	2.250	2.226
R_2 (a_0)	3.586	3.556	3.599	3.595
R_3 (a_0)	1.981	2.017	1.966	1.983
V (E_h)	−0.3568			−0.3568
ΔV^e (kcal/mol)	4.52	4.31[f]	3.8	4.52
ω_1(N−H) (cm^{-1})	2916	2577	2607	2887
ω_2(N−N) (cm^{-1})	1818	1931	1809	1862
ω_3(bend) (cm^{-1})	1118	1106	1137	1086
		Saddle Point for H + N$_2$ Reaction		
R_1 (a_0)	2.124	2.173	2.139	2.125
R_2 (a_0)	4.135	4.231	4.190	4.136
R_3 (a_0)	2.685	2.641	2.703	2.688
V (E_h)	−0.3399			−0.3399
ΔV^g (kcal/mol)	10.60	11.34[f]	11.4	10.60
ω_1(N−H) (cm^{-1})	1619i	1387i	1658i	1640i
ω_2(N−N) (cm^{-1})	2155	2027	1980	2102
ω_3(bend) (cm^{-1})	762	668	763	763
		Saddle Point for H−N$_2$ Isomerization		
R_1 (a_0)	2.324	2.390		2.326
R_2 (a_0)	2.285	2.291		2.281
R_3 (a_0)	2.285	2.291		2.281
V (E_h)	−0.2867			−0.2868
ΔV^g (kcal/mol)	48.51	51.6		48.44
ω_1(N−H) (cm^{-1})	2676			2753
ω_2(N−N) (cm^{-1})	1660			1668
ω_3(bend) (cm^{-1})	2278i			2295i

[a] From this work, from a fit to a Taylor-series-type expansion around the stationary point; see text. [b] From ref 8. [c] From ref 6. [d] This work. [e] Relative to the H + N$_2$ asymptote. [f] From ref 10; value extrapolated to the complete basis set limit. [g] Relative to the global minimum.

title system. A characterization of their attributes (geometry, energy, and vibrational frequencies) is reported in Table 5. Also included for comparison in this table are the results that have been obtained from other potential energy surfaces. Note that we have calculated a denser grid of energies in the vicinity of some stationary points which were then used to fit a local polynomial form to obtain an optimum prediction of the spectroscopic properties at the correlated ab initio level. Table
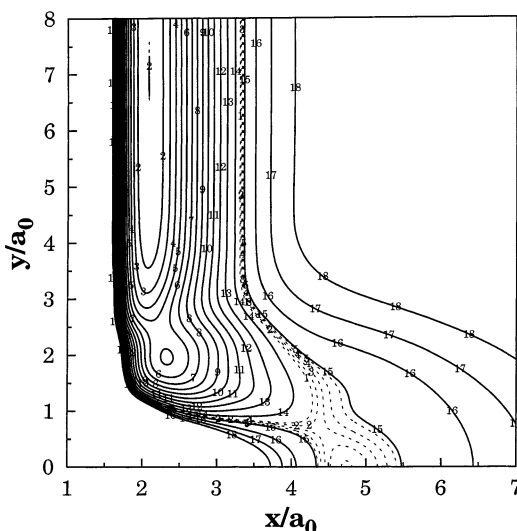
Figure 8. Isoenergy contour plot for the C_{2v} insertion of a H atom into a N$_2$ diatomic. Contours are equally spaced by 0.02 E_h, starting at -0.3641 E_h. Contours in dashed lines are equally spaced by 0.002 E_h, starting at -0.0932 E_h.

TABLE 6: Geometries and Energies of Other Important Stationary Points

property	van der Waals, H⋯N$_2$	linear TS N−H⋯N	linear TS N⋯H⋯N
R_1 (a_0)	2.076	6.379	4.740
R_2 (a_0)	7.231	1.943	2.370
R_3 (a_0)	7.231	4.436	2.370
V (E_h)	-0.3642	-0.1338	-0.0933
ΔV (kcal/mol)	-0.07^a	2.26^b	23.15^b
ω_1(N−H) (cm^{-1})	55	618	2163i
ω_2(N−N) (cm^{-1})	2335	4711	538
ω_3(bend) (cm^{-1})	14	138i	978

^{a} Relative to the H + N$_2$ asymptote. ^{b} Relative to the N + NH asymptote.

6 summarizes the properties obtained for other relevant stationary points, including the shallow van der Waals minimum in Figure 5 for intermediate H−N$_2$ distances.

Clearly, the current HN$_2$ DMBE potential energy surface provides an accurate representation of the properties of the global minimum and the two most important transition states: one that is associated with the reaction H + N$_2$ → NH + N, and another that is associated with the HN$_2$ isomerization process. Specifically, the barrier height for the process HN$_2$ → H + N$_2$ is predicted to be 10.6 kcal/mol before inclusion of the zero-point energy correction. Thus, it lies slightly below the 11.3 kcal/mol extrapolation of Walch and Partridge,[10] while being very similar to the result reported by Gu et al.[13] These authors have used an aug-cc-pVQZ basis set and the CCSD(T) method, having predicted a barrier height of 10.7 kcal/mol. As they also observed, experience suggests that such a barrier may be further reduced when larger basis sets and higher levels of theory are used.[8,13] The fact that our prediction lies slightly below the best-available theoretical estimates may then provide an indication that the DMBE−SEC method can reliably be used to extrapolate the ab initio energies to the complete basis set/configuration interaction limit.

We now turn to the global minimum, which is predicted in the present work to be 4.5 kcal/mol above the H + N$_2$ asymptote. Thus, it lies close to the Walch and Partridge[10] extrapolation of 4.31 kcal/mol and only slightly above the Gu et al.[13] prediction of 3.8 kcal/mol. This result may not be

surprising, because the literature shows that the estimated values for the barrier height have a tendency to show a more stable trend (∼11 kcal/mol) than the calculated exothermicity for the reaction HN$_2$ → H + N$_2$. We may attribute such a behavior to the fact that the exothermicity is dependent on the level of ab initio theory and basis set used in a more subtle way[3,8,10,13] (the best reported values cover the range of 3.0−5.6 kcal/mol). In fact, the calculated values reflect the dificulties that are usually encountered by the theoretical methods in describing both the short-range and long-range interactions in a balanced way.

The saddle point for the HN$_2$ isomerization process is located at a T-shaped configuration prior to the conical intersection, lying 48.5 kcal/mol above the H + N$_2$ asymptote. Both such features are visible in Figure 5, being located along the y-axis at ∼2.0 a_0. Thus, our estimated barrier height is somewhat smaller than the value of 51.6 kcal/mol that was reported by Walch,[8] which may have implications on the lifetime of the HN$_2$ metastable species.

As shown in Figure 5, the present calculations predict a C_{2v} van der Waals minimum with a well depth of 0.07 kcal/mol, relative to the H + N$_2$ asymptote. It is a very shallow minimum, which indicates an almost-free rotation of the H atom around N$_2$. Thus, in reality, the correct location of the lowest energy that is associated with such a weakly bound structure can hardly be warranted to correspond to a C_{2v}-type structure, despite the care taken in performing the least-squares fit and the appreciable number (46 in total) of ab initio points that have been calculated for $r_{H-N_2} \geq 6.5$ a_0.

Tables 5 and 6 show that the spectroscopic properties of all the stationary points in the DMBE potential energy surface are similar to the frequencies obtained when a Taylor-series-type expansion is instead used to fit a dense grid of energies in the vicinity of such points. Indeed, the average percentage error in the calculated frequencies is 1.0% for the global minimum, saddle point for the H + N$_2$ reaction, and saddle point for the HN$_2$ isomerization.

Figure 7 shows a contour plot for the linear N−H−N stretching. The main features are the two equivalent NH⋯N hydrogen-bond type structures, and the saddle point for the H-atom exchange process. Note that such structures are not true minima in three-dimensional configuration space, but rather are linear transition states, as indicated by the dashed contours in Figure 6. Indeed, they have a positive curvature with respect to NH⋯N stretching but a negative one with respect to bending. Table 6 summarizes the geometries, energies, and vibrational frequencies of such stationary points.

Finally, in Figure 8, we show a countor plot for the C_{2v} insertion of an H atom into N$_2$. Although the dashed contours might suggest the resulting linear configuration to be a minimum, it is indeed a saddle point, because it has a negative curvature with respect to the bending mode (H-atom insertion). In fact, such a "minimum" corresponds, in reality, to the saddle point that connects the two NH⋯N hydrogen-bond type structures that are observed in Figure 7. Also visible from Figure 8 is a shallow "minimum" located at $r_{H-N_2} \approx 2.0$ a_0, which is related to the saddle point that connects the two equivalent metastable structures shown in Figure 5. Finally, for large atom−diatom separations, we observe the very shallow H⋯N$_2$ van der Waals minimum that has been already discussed previously (see Figure 5 and Table 6).

5. Concluding Remarks

We have reported a single-valued DMBE potential energy surface for ground-state HN$_2$, on the basis of a realistic

7930 *J. Phys. Chem. A, Vol. 107, No. 39, 2003*

Poveda and Varandas

representation of the long-range forces and a fit to accurate ab initio calculations. The various topographical features of the new potential energy surface have been carefully examined and compared with previous calculations for the title system, most importantly, a potential energy surface that was previously reported by Walch and collaborators.[5,6,8,9] The geometries and spectroscopy of the main stationary points for the HN_2 global minimum, transition state for dissociation, and isomerization barrier height are reproduced very accurately when compared with the best available theoretical estimates. We emphasize that the predicted barrier height for dissociation lies below the best available estimates,[10,13] which suggests that the DMBE−SEC method offers a reliable means to extrapolate accurate correlated energies to the basis set/configuration interaction limit. Thus, we speculate that dynamics calculations that use the new potential energy surface are likely to predict a lifetime for the HN_2 species that is even shorter than previously reported estimates. Because the global minimum is predicted to lie 4.5 kcal/mol above the $H + N_2$ asymptote (which is slightly above the best estimates reported in the literature), we further argue that the stability of such a structure is yet unresolved, although it definitely seems to be a metastable one. To summarize, the DMBE potential energy surface reported in the present work is globally valid and accurately fits our ab initio calculations and, for that reason, is being recommended for future dynamics studies of the $H + N_2 \rightarrow HN_2 \rightarrow HN + N$ reaction.

References and Notes

(1) Miller, J. A.; Branch, M. C.; Kee, R. J. *Combust. Flame* **1981**, *81*, 43.

(2) Miller, J. A.; Bowman, C. G. *Prog. Energy Combust. Sci.* **1989**, *15*, 287.

(3) See ref 5 and references therein.

(4) Glarbor, P. G.; Miller, J. A.; Kee, R. J. *Combust. Flame* **1986**, *177*, 65.

(5) Walch, S. P.; Duchovic, R. J.; Rohlfing, C. M. *J. Chem. Phys.* **1989**, *90*, 3230.

(6) Koizumi, H.; Schatz, G. C.; Walch, S. P. *J. Chem. Phys.* **1991**, *95*, 4130.

(7) Guo, Y.; Thompson, D. L. *J. Chem. Phys.* **2002**, *116*, 3670.

(8) Walch, S. P. *J. Chem. Phys.* **1990**, *93*, 2384.

(9) Walch, S. P. *J. Chem. Phys.* **1991**, *95*, 4277.

(10) Walch, S. P.; Partridge, H. *Chem. Phys. Lett.* **1995**, *233*, 331.

(11) Dunning, T. H., Jr. *J. Chem. Phys.* **1989**, *90*, 1007.

(12) Kendall, R.; Dunning, T., Jr.; Harrison, R. *J. Chem. Phys.* **1992**, *96*, 6769.

(13) Gu, J.; Xie, Y.; Schaefer, H. F., III. *J. Chem. Phys.* **1998**, *108*, 8029.

(14) Varandas, A. J. C. *J. Mol. Struct. Theochem.* **1985**, *120*, 401.

(15) Varandas, A. J. C. *Adv. Chem. Phys.* **1988**, *74*, 255.

(16) Varandas, A. J. C. *Chem. Phys. Lett.* **1992**, *194*, 333.

(17) Varandas, A. J. C. *Lecture Notes in Chemistry*; Laganá, A., Riganelli, A., Eds.; Springer: Berlin, 2000; Vol. 75, p 33.

(18) Varandas, A. J. C. *J. Chem. Phys.* **1989**, *90*, 4379.

(19) Werner, H.-J.; Knowles, P. J. *J. Chem. Phys.* **1988**, *89*, 5803.

(20) Knowles, P. J.; Werner, H.-J. *Chem. Phys. Lett.* **1985**, *115*, 259.

(21) Werner, H.-J.; Knowles, P. J. MOLPRO, 1998. (MOLPRO is a package of *ab initio* programs written by H.-J. Werner and P. J. Knowles, with contributions from J. Almlöf, R. D. Amos, M. J. O. Deegan, S. T. Elbert, C. Hampel, W. Meyer, K. A. Peterson, R. Pitzer, A. J. Stone, P. R. Taylor, and R. Lindh.)

(22) Varandas, A. J. C.; Silva, J. D. *J. Chem. Soc. Faraday Trans.* **1992**, *88*, 941.

(23) Varandas, A. J. C. *Mol. Phys.* **1987**, *60*, 527.

(24) Le Roy, R. J. *Mol. Spectrosc. (Chem. Soc. London)* **1973**, *1*, 113.

(25) Edwards, S.; Roncin, J.; Launay, F.; Rostas, F. *J. Mol. Spectrosc.* **1993**, *162*, 257.

(26) Varandas, A. J. C.; Rodrigues, S. P. J. *J. Chem. Phys.* **1997**, *106*, 9647.

(27) Stallcop, J. R.; Bauschlicher, C. W., Jr.; Partridge, H.; Langhoff, S. R.; Levin, E. *J. Chem. Phys.* **1992**, *97*, 5578.

(28) Varandas, A. J. C. *J. Chem. Phys.* **1996**, *105*, 3524.

(29) Varandas, A. J. C.; Rodrigues, S. P. J. *Chem. Phys. Lett.* **1995**, *245*, 66.

(30) Matías, M. A.; Varandas, A. J. C. *Mol. Phys.* **1990**, *70*, 623.

(31) Martínez-Nuñez, E.; Varandas, A. J. C. *J. Phys. Chem.* **2001**, *105*, 5923.